

RESEARCH OF EFFECTS OF DEFECTS ON STABILITY FAILURES OF SEMI-MONOCOQUE STIFFENERS

Tomáš KATRŇÁK *, Jaroslav JURAČKA , Ivo JEBÁČEK 

*Institute of Aerospace Engineering, Faculty of Mechanical Engineering,
Brno University of Technology, Brno, Czech Republic*

Received 28 February 2019; accepted 23 December 2019

Abstract. This article presents further results of the research of effects of model defects on the local buckling of compressed stiffeners in nonlinear finite element (FE) analyses. The main outcomes are confirmation of trends for 10 sets of profile dimensions, final validations of various sets of FE simulations, and designs of practical types of defects with appropriate ratio values. A single node defect and then complex types of defects with alternating distributions of node shifts along one edge, two free flange edges, one flange surface and both flange surfaces are analyzed in this research project. First parts of this paper describe designed FE models with defects, their effects on simulation results, colored graphic visualizations with stress scales and determinations of the sudden failure of stability in the local mode. Then, particular results of FE analyses are validated by a comparison with the results of analytical methods of stability failure. Final detail comparisons of analytical and FE simulation results with data of experimental tests confirm predicted critical buckling forces. The validation of results and design parameters together with the knowledge of effects of model defects on buckling behaviors allows more accurate simulations of internal stiffeners of thin-walled semi-monocoque structures.

Keywords: buckling, stability, failure, stress analysis, finite element methods, stiffener, imperfection.

Introduction

Problems of effect of defects on buckling behaviors of semi-monocoque aircraft structures in advanced finite element analyses are at the forefront of many research institutions. The knowledge of effects and appropriate values of defects is necessary for the proper determination of the total load capacity of complex semi-monocoque structures with the use of numeric simulations. This knowledge can be also utilized for the following predictions of buckling failures, where accurate diagrams for a safe design are not available. General theories of stability failures of thin-walled flight vehicle structures are described by Hoff (1967) and Bruhn (1973). The comprehensive reviews on stability behaviors of compressed stiffeners in aerospace structures are presented in Niu (1999), from which an analytical approach of determination of critical buckling forces was used. Among with the survey articles, which deal specifically with the buckling and post-buckling theory, belong Ortiz and Martinez (2001) or Degenhardt, Tessmer, and Kling (2008). Detailed articles with a direct method design are presented by Batista (2009a), (2009b). The study Chen (2014) of imperfection types confirmed

the necessity of defect application in FE models. The paper by Symonov and Katrňák (2013) contributed to a comparison of nonlinear FE analyses and analytical approaches. Analytical solutions of skin buckling and effects of stiffener torsional and warping failures and the verification by finite element methods are presented in the study by Soares et al. (2013). The complementary research was found in research papers by Horák and Píštěk (2016), Pravdová and Eliášová (2017). Measurement techniques and test procedures of aircraft structural parts are described in the paper by Jebáček and Matějů (2017). This scientific article continues in the research of effects on buckling behaviors and determination of appropriate imperfections. The complex research was done at Brno University of Technology and, therefore, student participation in basic research was allowed. Students assisted under supervision with finite element analyses of buckling sensitivity on applied imperfection. Initial results of buckling analyses were presented in the student's bachelor thesis Hála (2017), which was awarded by the Bosch prize in 2017. The initial overview of this research of only one set of profile dimensions was published in Katrňák and Juračka (2018). This following

*Corresponding author. E-mail: katrnak@fme.vutbr.cz

article presents a significantly advanced description of complemented research, which was done additionally to observe detail effect of following types of stiffener defects and dimensions. The detail validation of FEA results with analytical methods and results of experimental tests is also an important part of this paper.

1. Model and simulations

For this research and numeric simulations the finite element models of a typical aircraft structural profile with the cross-sectional L shape and equal flanges were created. The first set of stiffener dimensions consisted of a flange width 20 mm and flange thickness 1 mm. This specific set represented a model of the stiffener L20×20×1.0 for initial FE simulations. This research was enhanced to 10 sets in total of outer dimensions by stiffeners L15×15×1.0, L20×20×0.8, L20×20×1.1, L20×20×1.2, L20×20×1.5, L20×20×1.67, L20×20×2.0, L20×20×2.5 and 30×30×3.0. The geometry specifications of all of these stiffener sets are listed in Table 1. Behaviors and effects on buckling are presented with the use of the set L20×20×1.0 in following chapters of this article for uniform presentation of results. Evaluations of other sets are also included in the final chapters of this paper. All models had a length equal to 80 mm to adjust FE models for a simulation of the local buckling behavior.

The typical discretization of FE model with three elements in the height of profile flange for buckling analyses with imperfection is presented in Figure 1. This coarse mesh was used on purpose to reduce an amount of elements and evaluation of its effect on buckling. These types of semi-monocoque stiffeners are the essential members of wing or fuselage structures and the number of elements in the entire FE models significantly affects the time of detail nonlinear FE analyses. Therefore, the coarse mesh is preferred and the mesh convergence test was done with two, three and four elements in the flange height. Two elements were not sufficient for the appropriate failure simulations. Three and four elements in the height of pro-

file flange were sufficient, but four elements increased the time of computation and post-processing. Therefore, the optimal solution is the discretization of FE models with three elements in the height of profile flange. Also testing simulations with 1D, 2D and 3D element types, and comparison of sensitivity of models and the time consumption of simulations were done. Based on these results, the standard shell elements CQUAD4 were utilized in following models.

The one side of the specimen model was fully clamped with the multipoint connector RBE2, which allowed direct evaluation of reaction buckling force (translational constraint force). The second end of the model was loaded with the multipoint connector RBE2 for fast and even distribution of the specimen shortening with the maximum value 0.5 mm, which was split to 50 steps with the equal difference 2% of load (0.01 mm). The homogenous metal material Duralumin 2024 with the yield stress $R_p 0.2 = 290$ MPa, strength limit stress $R_m = 440$ MPa, Young's modulus $E = 72.4$ GPa and elastoplastic properties with the hardening modulus slope $H = 942$ MPa was applied in FE model. The structural analysis was computed in the MSC.MD Nastran 2017.1 software, which enables to use nonlinear buckling behaviors for large deformations. The nonlinear static solution sequence 106, automatic matrix update method with 50 equal load steps and 25 allowable iterations per increment were used. A post-processing procedure in MSC.Patran software transformed result from MSC.Nastran database to a report file, which was processed in Excel software.

2. Evaluation of effect of imperfection A

The purpose of this research is to find the appropriate combinations of coarse mesh model and simple imperfection types to reduce the time of modelling, nonlinear FE simulations and post-processing. The first set of FE models with applied imperfections in the one middle node of length of the profile flange was marked as the imperfection A and it is displayed in Figure 1.

Table 1. Specification of stiffener geometry characteristics

Stiffener specification	Flange 1 length b_1	Flange 2 length b_2	Flange 1 thickness t_1	Flange 2 thickness t_2	Stiffener length L	Cross-section area A
[-]	[mm]	[mm]	[mm]	[mm]	[mm]	[mm ²]
L15×15×1.0	15.0	15.0	1.0	1.0	80.0	29.0
L20×20×0.8	20.0	20.0	0.8	0.8	80.0	31.4
L20×20×1.0	20.0	20.0	1.0	1.0	80.0	39.0
L20×20×1.1	20.0	20.0	1.1	1.1	80.0	42.8
L20×20×1.2	20.0	20.0	1.2	1.2	80.0	46.6
L20×20×1.5	20.0	20.0	1.5	1.5	80.0	57.8
L20×20×1.67	20.0	20.0	1.67	1.67	80.0	63.9
L20×20×2.0	20.0	20.0	2.0	2.0	80.0	76.0
L20×20×2.5	20.0	20.0	2.5	2.5	80.0	93.8
L30×30×3.0	30.0	30.0	3.0	3.0	80.0	171.0

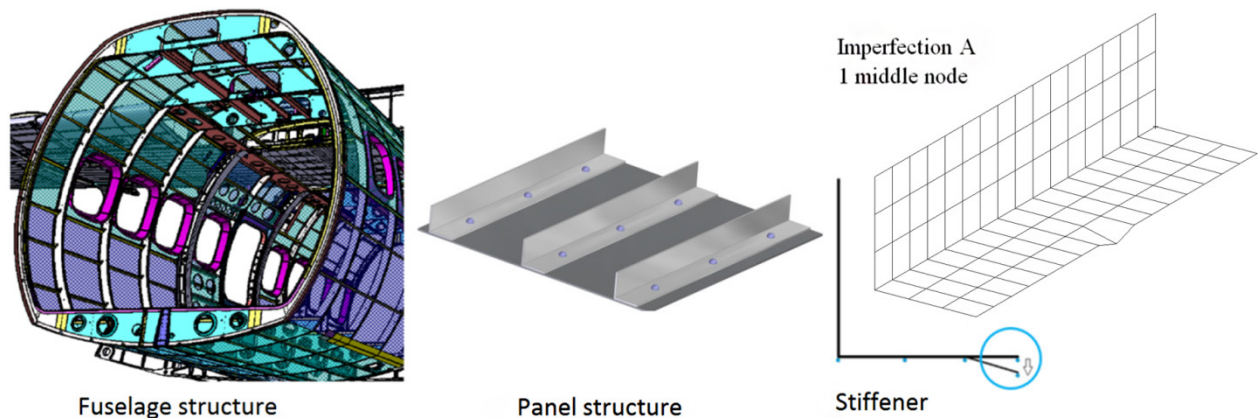


Figure 1. Practical example of semi-monocoque fuselage structure, panel structure and FE model of the particular stiffener with imperfection A

Specific distributions of induced compression force per shortening of the profile L20×20×1.0-80 are presented in Figure 2, where is showed that all force distributions have identical model stiffness up to particular points of buckling instability. Peaks of force distributions after the initial linear part represent critical buckling forces, where model stability failed. These critical buckling forces were compared with the critical force and its tolerance range, which was obtained from evaluation of experimental tests.

The trend in effects of imperfection can be observed in Figure 2, where an increase of imperfection value caused a decrease of buckling forces. Numeric results comparison of buckling forces and corresponding cross-section average stresses before the failure of stability are listed in Table 2. The peak of the force distribution of the profile L20×20×1.0-80 with the ratio of imperfection per flange thickness e/t equal to 0.05 for this initial set of imperfection A has the nearest approach to the critical buckling force from experimental tests. The simulated buckling force has higher value with a force difference +0.8%. Therefore, the next ratio of imperfection per flange thickness e/t equals to 0.10 for this initial set of imperfection A was evaluated as the most suitable ratio of imperfection with the safe reserve value -4.7% of buckling force.

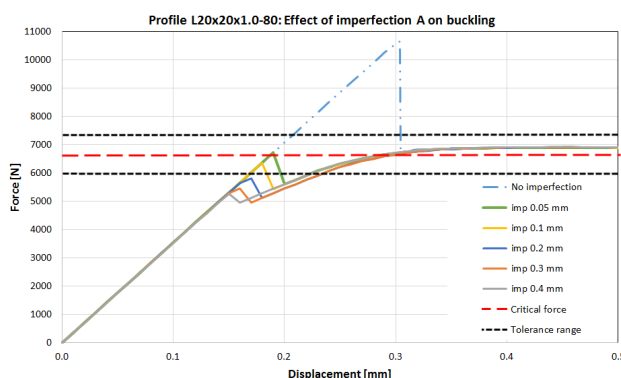


Figure 2. Graphic comparison of force distributions per model displacement

Many particular sets of colored graphic visualizations with stress scales were evaluated. The sudden failure of stability in the local mode for a model with the imperfection A equal to ratio $e/t = 0.05$ is presented in Figure 3. The stable level at 38% of load is depicted on the left part of Figure 3 and the significant change to the buckled mode at 40% of load on the right figure part. These graphic visualizations allow detail investigation of von Mises stress distributions (maximum stress of 2 element layers) in FE models. The maximum evaluated von Mises stress at the moment before buckling is 191 MPa, minimum von Mises stress is 151 MPa and average buckling stress level is 172 MPa.

Table 2. Numeric comparison of buckling force and buckling stress results – effect of imperfection A

Imperfection [mm]	Ratio e/t [-]	Buckling force [N]	Average buckling stress [MPa]
0.00	0.00	10652	273
0.05	0.05	6725	172
0.10	0.10	6368	163
0.20	0.20	5824	149
0.30	0.30	5462	140
0.40	0.40	5260	135

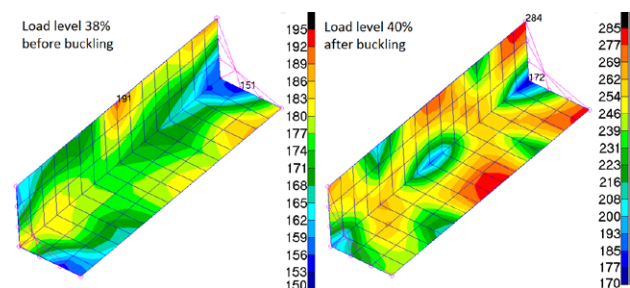


Figure 3. Graphic visualization of von Mises stress distributions on FE model with imperfection A

Generally, these typical aircraft structural profiles with the cross-sectional L shape can have multiple buckling modes. The global and local buckling failures can be classified according to papers by Wang and Abdalla (2015) or Niu (1999). The all presented stiffener sets have short lengths and low slenderness values to observe effects of defects on the local buckling mode of semi-monocoque stiffeners.

3. Evaluation of effects of complex types of imperfections

Next sets of imperfections were designed analogically according to evaluations of the initial set with imperfection A. The second FE model set with imperfection B contained alternating distribution of node imperfections with 5 dimensions along the one flange edge. This model is showed in Figure 4. The next set with imperfection C had alternating distributions of node shifts along two free flange edges. Colored graphic visualizations of von Mises stress distribution (maximum stress of 2 element layers) on FE model of the profile L20×20×1.0-80 with imperfection C equal to the ratio $e/t = 0.3$ are depicted in Figure 5.

Following two sets with imperfections D and E, presented in Figure 6, were designed with alternating node imperfections on entire one flange surface and both flange surfaces. All of these models were computed and evaluated according to designed procedure.

Colored graphic visualizations of von Mises stress distributions (maximum stress of 2 element layers) before and after the failure of stability for the imperfection E equal to the ratio $e/t = 0.3$ are depicted in Figure 7. The von Mises stress distribution (maximum stress of 2 element layers) on model of the profile L20×20×1.0-80 at the stage before buckling shows the load is transferred through the middle part of the model along the connection of both stiffener flanges.

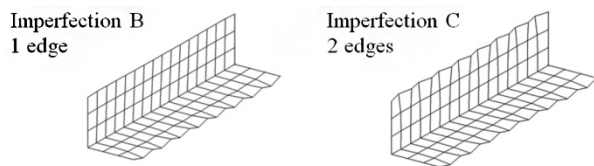


Figure 4. FE models of particular sets of imperfections B and C

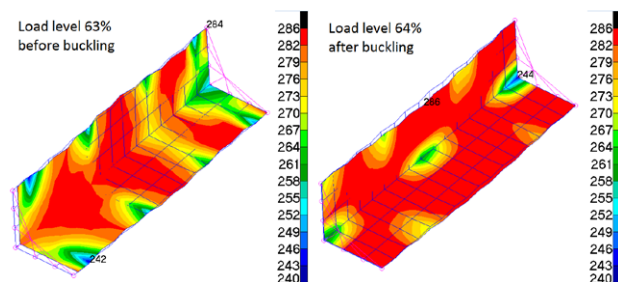


Figure 5. Graphic visualization of von Mises stress distribution on FE model with imperfection C

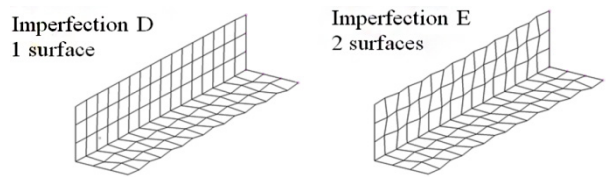


Figure 6. FE models of additional sets of imperfections D and E

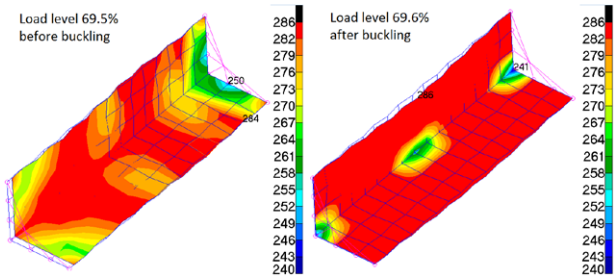


Figure 7. Graphic visualization of von Mises stress distribution on FE model with imperfection E

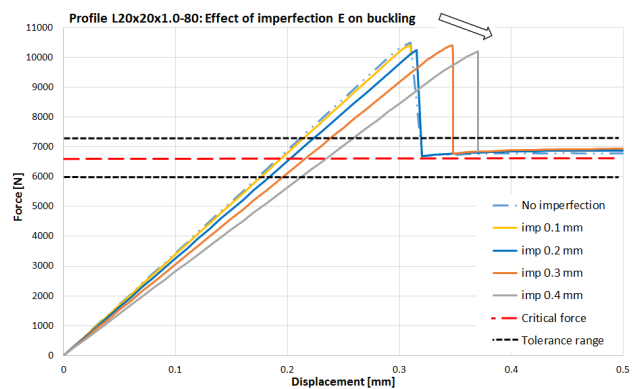


Figure 8. Graphic comparison of force distributions per model displacement for imperfection E

Detail comparisons of distributions of induced compression force per profile shortening is presented in Figure 8. Applied imperfections on both flange surfaces caused significant changes of model stiffnesses up to particular points of buckling instability. All peaks of force distributions, representing critical buckling forces, have higher values than the critical force and its tolerance range, which was obtained from evaluation of experimental tests. All evaluated critical buckling forces are out of the tolerance range 10%, therefore, this type of imperfection E is not recommended for simulations. The arrow in Figure 8 presents the trend in effects of defect values.

4. Final evaluation of results of FE analyses

The various sets of imperfection types were evaluated with the comparison of force distribution per model displacement and the necessity of defect application in models was confirmed. All local buckling failures were simulated in elastic range with the von Mises stresses lower than the defined yield stress. An increasing dimension of defect

decreased the peak of force distribution and the buckling instability appeared at lower load levels. The ratio e/t value 0.10 was evaluated as the most suitable defect ratio with a safe reserve for a set of imperfection A of the profile L20×20×1.0-80. Also the ratio $e/t = 0.10$ was evaluated as the optimal value for the set of imperfection B of this specific profile. The imperfection C and E are not recommended for simulations due to a significant decrease of model stiffness and results out of the tolerance range. The optimal defect ratio for the set of imperfection D of the profile L20×20×1.0-80 was evaluated equal to ratio 0.20. Trend comparisons in Hála (2017) for the profile L15×15×1.0-80 and evaluations of following research of other eight sets of outer profile dimensions presented similar trends in effects of defect types. Only the optimal defect ratios were different for the each specific combination of sets of imperfection and outer stiffener dimensions.

5. Results of analytical methods

The results of FE analyses were compared with results of analytical methods of global, local and transition regions of the critical stability failures. The classifications of global and local failures were found in Niu (1999), Wang and Abdalla (2015). The determination of critical failure by analytical methods is described in detail in Hála (2017). The critical global buckling stress was derived by the Euler’s formula, which describes a global flexural failure of entire stiffener volume.

$$\text{Global buckling stress: } \sigma_{GLOBALi} = \frac{c_i \pi^2 E J_i}{A_i L_i^2}. \quad (1)$$

Then, the critical local buckling stress was determined for protruded profiles according to methods presented by Niu (1999). Other local buckling stresses were calculated by diagrams designed by Timoshenko and Bruhn, only for additional comparison. These local buckling stresses are dependent only on profile cross-section and independent on profile length.

$$\text{Local buckling stress: } \sigma_{LOCALi} = K_i E \left(\frac{t_i}{b_i} \right)^2. \quad (2)$$

The final determination of critical failure of stability in transition region including real length of profile was made according to the Johnson’s method, found in Niu (1999).

$$\text{Specimen slenderness: } \lambda_i = \frac{L_i}{\sqrt{c_i \frac{J_i}{A_i}}}; \quad (3)$$

$$\text{Threshold slenderness: } \lambda_{Ti} = \sqrt{\frac{2\pi^2 E}{\sigma_{LOCALi}}}; \quad (4)$$

Buckling stress in transition:

$$2(1 + \cos \delta) \left(u - \frac{l}{2} \right)^2 + l^2 \sin^2 \frac{\delta}{2}. \quad (5)$$

The specimen characteristics of the representative stiffener profile L20×20×1.0 are presented in Table 3 and following profiles can be calculated analogically. The profile L20×20×1.0 with the length 80 mm has a low slenderness equal to 12.8 and threshold slenderness is 93.4. Therefore, the critical buckling stress in transition region was calculated equal to 161 MPa, according to formula (5).

6. Results of experimental tests

The following step was the evaluation of experimental test data. The set of experimental laboratory tests was done during previous researches at Institute of Aerospace Engineering at Brno University of Technology. The eight identical stiffener specimens were tested for the determination of one particular stiffener behavior. The all specimen dimensions and shape curvatures were measured before testing. The detected geometry values were in the required standard tolerances and these stiffener specimens represent the real quality of manufacturing. The tests were performed on the electro-hydraulic test machine ZUZ 200, equipped with the digital regulators of power unit and GTM force meters with the maximal force of 250 kN. This test device had the valid calibration and was certified by Civil Aviation Authority Czech Republic. The accuracy of the measurement device is 0.1% and the maximal sample frequency is 200000 samples per second. The both test specimens endings were aligned by precise milling procedure and attached in vertical position between the upper and lower load units to provide the simply supported boundary conditions. The typical loading velocity 1.5 mm/min compressed specimens up to the stability failures. The recorded compression force and deformation values were evaluated in detail. The arithmetic mean and standard deviation values were derived from the force-displacement distributions of all eight measurements in stiffener sets by the standard statistic methods. The detail description of the measured geometry values and the process of evaluation of statistic results are not the main purpose of this scientific paper. The final average buckling stress values from experimental tests are listed in Table 4. The critical buckling test force equal to 6669 N and critical buckling test stress 171 MPa for the profile L20×20×1.0-80 were evaluated from the average force distribution as the maximum force at the moment of a buckling failure.

Table 3. Specification of stiffener geometry and mechanical characteristics

Stiffener specification	Ratio b/t	Specimen slenderness λ	Threshold slenderness λ_T	Global buckling stress σ_{GLOBAL}	Local buckling stress σ_{LOCAL}	Buckling stress in transition σ_{TRAN}
[-]	[-]	[-]	[-]	[MPa]	[MPa]	[MPa]
L20×20×1.0	20.0	12.8	93.6	4359	163	161

7. Validation with results of analytical methods and experimental tests

The particular results of FE analyses with nonlinear behaviors of structural stability were validated by the final detail comparison with results of analytical methods and experimental tests. The detail comparison of force distributions per model displacement of all five sets of imperfection was done with uniform ratio e/t value 0.1 in Figure 9. This ratio value was selected for the determination of differences and effects of imperfection types on buckling behaviors. The critical value of buckling test force and the value of critical buckling force of Johnson's approach for transition region were also added into this Figure 9.

The FE simulation with the imperfection A was evaluated as the most suitable type of imperfection due to the best safe approach of the buckling failure to the critical buckling force derived from experimental tests. These behaviors are presented in the detail comparison of force distributions in Figure 9. An identical effect was observed also for other designed sets of stiffener dimensions, therefore, the imperfection A is recommended as the optimal defect for a modification of FE models of thin-walled metal stiffeners and their simulations of stability failures. Also the buckling modes of the simulations of FE models with the imperfection A and failure modes of stiffeners at experimental tests were very similar and corresponded to classification of the local buckling failures according to papers by Wang and Abdalla (2015), Niu (1999). The example of locally buckled specimen is presented in following Figure 10. The evaluation of failure modes is also the very important factor for the validation of simulated and tested results.

The optimal defect ratios for this imperfection type A were evaluated for all 10 sets of specific outer stiffener dimensions. The appropriate ratio values of defects applied in models for nonlinear finite element analyses are depicted in Figure 11 and listed in Table 4. The ratio b/t represents a proportion of outer profile dimensions, where quantity b is the height and t is the thickness of profile

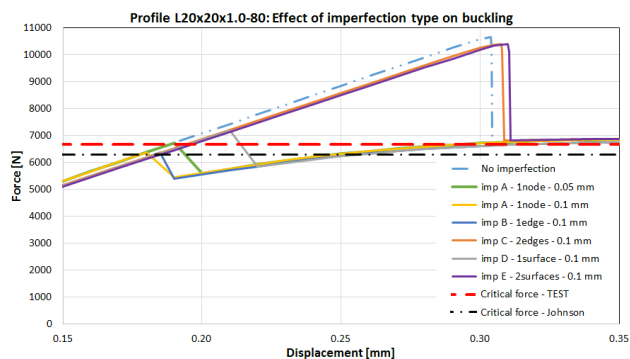


Figure 9. Final graphic comparison of force distributions for all types of imperfections



Figure 10. Example of failed stiffener test specimen in local buckling mode

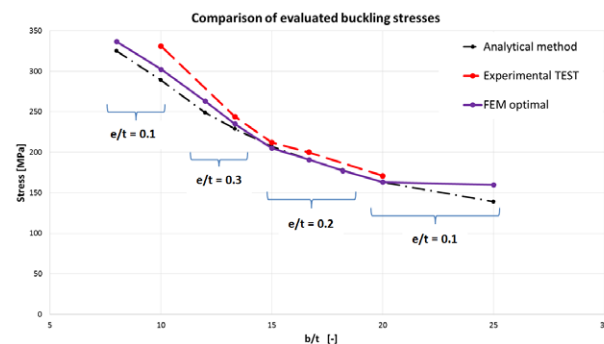


Figure 11. Complex comparison of results of various sets profile dimensions

Table 4. Comparison of results gained by analytical methods and experimental tests

Stiffener	Analytical method	Experimental TEST	FEM optimal	Ratio of imperfection
Ratio b/t	Buckling stress in transition	Buckling stress from test	Buckling stress from FEA	Ratio e/t
[-]	[MPa]	[MPa]	[MPa]	[-]
8.0	324	-	337	0.1
10.0	288	331	303	0.1
12.0	248	-	263	0.3
13.3	228	244	235	0.3
15.0	205	212	205	0.2
16.7	191	200	191	0.2
18.2	177	-	177	0.2
20.0	161	171	161	0.1
25.0	138	-	159	0.1

flange. The final detailed validation of the particular results of FE analyses with the imperfection type A (FEM optimal) by the results of analytical methods and experimental tests is presented in Table 4. For the range of ratios b/t from 8 to 10 the optimal ratio of imperfection per flange thickness e/t equals to 0.10. The ratio $e/t = 0.30$ is recommended for the range b/t from 12 to 14. Then, the ratio $e/t = 0.20$ was evaluated as the best for the range b/t from 15 to 18 and ratio $e/t = 0.10$ for the range b/t from 20 to 25.

Conclusions

The final validations of various sets of imperfection types confirmed the necessity of defect application in FE models where natural curvature of structures is not sufficient. The imperfection type A was evaluated as the most suitable type of defect for this design of stiffener model. Main outcomes of this research of effect of model defects on the local buckling of compressed stiffeners in nonlinear FE analyses are the practical ratio values of defects recommended for the wide range of specific stiffener dimensions. This improvement in FE simulations and evaluations of critical failures of structural elements of thin-walled semi-monocoque structures allows more accurate predictions of behaviors of complex aircraft structures under an applied outer load and a final weight reduction of designed structure.

Funding

These outputs were supported by the project TE02000032 – Advanced Aerostructures Research Centre. This project was realized with financial support from national budget of the Technology Agency of the Czech Republic.

Author contributions

TK conceived the study and was responsible for the design and development of the data analysis. TK, JJ and IJ were responsible for analysis and writing of the article.

Disclosure statement

Authors do not have any competing interests from other parties.

References

- Batista, E. de M. (2009a). Local–global buckling interaction procedures for the design of cold-formed columns: Effective width and direct method integrated approach. *Thin-Walled Structures*, 47, 1218–1231.
<https://doi.org/10.1016/j.tws.2009.04.004>
- Batista, E. de M. (2009b). Stability of steel cold-formed columns and beams: Integrating effective width and direct strength methods for design. In *Proceedings of the 7th EUROMECH Solid Mechanics Conference 2009* (pp. 665–668). Lisbon, Portugal.

- Bruhn, E. F. (1973). *Analysis and design of flight vehicle structures*. Carmel: Jacobs Publishing, Carmel, USA.
- Degenhardt, R., Tessmer, J., & Kling, A. (2008). Collapse behaviour of thin-walled CFRP structures due to material and geometric nonlinearities – experiments and simulation. In *Proceedings of the 26th International Congress of the Aeronautical Sciences ICAS 2008* (pp. 1–10). Anchorage, Alaska, USA.
- Hála, A. (2017). *Stability analysis of metal stiffeners under compressive load using finite element methods* (Bachelor thesis). VUT v Brně, Brno, Czech Republic (in Czech).
- Hoff, N. J. (1967). Thin shells in aerospace structures. *Journal of Astronautics and Aeronautics*, 5(2), 26–45.
- Horák, M., & Pištěk, A. (2016). Shear strength of thin web – influence of lighting openings and diagonal tension. *Aviation Journal*, 20(1), 8–13.
<https://doi.org/10.3846/16487788.2016.1168008>
- Chen, T. (2014). *On introducing imperfection in the non-linear analysis of buckling of thin shell structures* (Master thesis). TU Delft, Delft, Netherland.
- Jebáček, I., & Matějů, J. (2017). Aerobatic special in-flight tests at Institute of Aerospace Engineering. In *Proceedings of the 23rd International Conference Engineering Mechanics 2017* (pp. 42–45). Svratka, Czech Republic.
- Katrnák, T., & Juračka, J. (2018). Buckling analyses of compressed stiffener with finite element methods. In *Proceedings of the 24th International Conference Engineering Mechanics 2018* (pp. 373–376). Svratka, Czech Republic.
- Niu, M. C. Y. (1999). *Airframe stress analysis and sizing: Practical design information and data on aircraft* (2nd ed.). Hong Kong Conmilit Press.
- Ortiz, S. S., & Martinez, A. A. (2001). Validation of post-buckling behaviour of unstable cross-section structures under compression loads. In *Proceedings of the 3rd Worldwide Aerospace Conference and Technology Showcase 2002* (pp. 1–16). Toulouse, France.
- Pravdová, I., & Eliášová, M. (2017). Influence of an initial imperfection on the lateral and torsional buckling of a hybrid beam. In *Proceedings of the 23rd International conference Engineering Mechanics 2017* (pp. 802–805). Svratka, Czech Republic.
- Soares, P. T. M. L., Monteiro, F. A. C., Neto, E. L., & Bussamra, F. L. S. (2013). Skin buckling of fuselages under compression. In *Proceedings of the 22nd International Congress of Mechanical Engineering COBEM 2013*.
- Symonov, V., & Katrnák, T. (2013). FEM approach to estimate large deformations of stiffened fuselage structure. In *Proceedings of the New Trends in Civil Aviation 2013* (pp. 90–92). Žilina, Slovak Republic.
- Wang, D., & Abdalla, M. M. (2015). Global and local buckling analysis of grid-stiffened composite panels. *Composite Structures*, 119, 767–776.
<https://doi.org/10.1016/j.compstruct.2014.09.050>

Notations

Variables and functions

- A – cross-section area [mm^2];
 b – stiffener flange length [mm];
 c – column end fixity coefficient [–];
 E – Young's modulus [MPa];
 e – imperfection value [mm];
 e/t – ratio of imperfection per flange thickness [–];
 F – buckling force [N];

H – hardening modulus slope [MPa];
 i – item number in index [-];
 J – second moment of area [mm⁴];
 K – compression attachment coefficient [MPa];
 L – stiffener length [mm];
 R_m – strength limit stress [MPa];
 $R_{p0.2}$ – yield stress [MPa];
 t – flange or element thickness [mm];
 σ – normal stress (general) [MPa];
 σ_{GLOBAL} – global buckling stress [MPa];
 σ_{LOCAL} – local buckling stress [MPa];
 σ_{TRAN} – buckling stress in transition [MPa];
 λ – specimen slenderness [-];
 λ_T – threshold specimen slenderness [-];

Abbreviations

RBE2 – Rigid Body Element – Form 2
CQUAD4 – Quadrilateral Plate Element Connection with
Four Grid Points
FE – Finite Element
FEM – Finite Element Method
FEA – Finite Element Analysis